Journal of Sol-Gel Science and Technology (2023) 107:201–214
https://doi.org/10.1007/s10971-023-06112-y

INVITED PAPER: SOL–GEL, HYBRIDS AND SOLUTION CHEMISTRIES

Transition metal-modification of carrageenan-silica hybrids by a sol–gel method

Sofia F. Soares[1] · Ana L. Daniel-da-Silva[1] · Tito Trindade[1]

Received: 16 December 2022 / Accepted: 7 April 2023 / Published online: 29 April 2023

Abstract

Transition metal (TM)-modification of silica matrices are found in numerous materials for diverse applications. In other related hybrid materials, one tries to explore properties that result from combining the silica network with organic moieties, such as in the covalent grafting of polysaccharides onto amorphous nanosilicas. However, sol–gel routes for modification with TM have been less explored for hybrid siliceous materials. The present study demonstrates the effective modification of hybrid siliceous materials with TM (TM = Co^{2+}, Ni^{2+}, Cu^{2+}, Zn^{2+}) that result from a sol–gel method that uses as a precursor the polysaccharide κ-carrageenan that was modified with a covalently alkoxysilane linked. Structural analysis and characterization studies of the derived carrageenan-silica hybrids were undertaken, and, in particular, the effects of the TM ions on the hybrids' properties have been assessed. This work clearly indicates that the modification with TM imposes changes on the morphological, optical, and thermal properties of the hybrids compared to the unmodified analogs. Hence, the practical applicability of the modification with TM using the sol–gel described here is not limited to the presence of the guest ion but also provides a tool for changing the properties of the host particles.

Graphical Abstract

Well-defined spheroidal shape κ-carrageenan silica particles doped with transition metals (Co^{2+}, Cu^{2+}, Ni^{2+}, and Zn^{2+}) prepared using a sol–gel method.

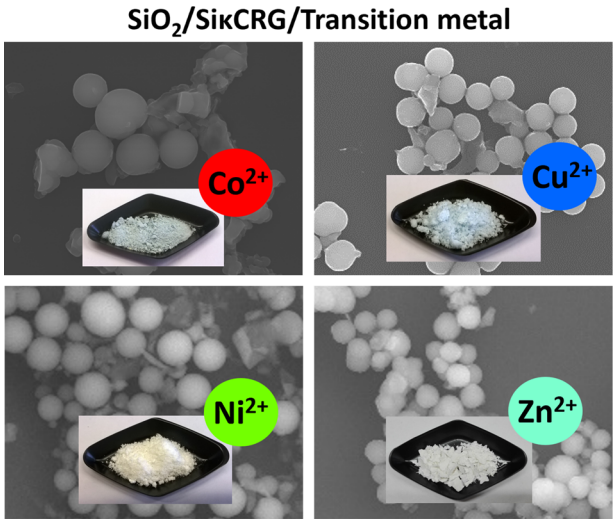

Supplementary information The online version contains supplementary material available at https://doi.org/10.1007/s10971-023-06112-y.

✉ Sofia F. Soares
sofiafsoares@ua.pt

[1] CICECO-Aveiro Institute of Materials, Department of Chemistry, University of Aveiro, 3810-193 Aveiro, Portugal

Keywords Organic–inorganic hybrids · Transition metal · Carrageenan · Silica · Sol–gel

Highlights

- Transition metal (TM) doped carrageenan-silica hybrids were prepared using a sol–gel method.
- The synthetic strategy reported does not require surfactants as templates.
- Hybrid particles of greater monodispersity and well-defined spheroidal shape have been obtained.
- TM doping changes the morphological, optical, and thermal properties of the hybrids compared to the non-doped analogs.

1 Introduction

The incorporation of transition metal ions in silica-based materials is well known and is part of technologies widely used in the manufacture of glass materials for various applications [1–3]. The exchange of silicon sites in the silica network with ions of Co(II) in a tetrahedral environment imparts the well-known cobalt-blue color that can be appreciated in several decorative glasses [4]. Colored silica gel, commonly used as a desiccant, also contains Co(II) as a colorimetric indicator and rare-earth ions (e.g., Er^{3+}) doping of silica glass optical fibers are explored for signal amplification in telecommunications [3], among many other examples of technological relevance. In this regard, sol–gel routes are quite effective for homogeneous doping because the metal guest species are incorporated within the host as the silica network is formed due to a series of hydrolytic and condensation reactions of silica oligomers [5]. The adaptation of such metal doping methodologies to the fabrication of hybrid biomaterials is not straightforward, namely because of the challenges associated with using different types of building blocks in the fabrication of such materials and their influence on the coordination chemistry involved. For example, in using polysaccharides as the organic component in siliceous hybrid materials, the metal coordination environments that result depend on the metal ion exchange of silicon sites and the metal chemical affinity for functional groups existent in the organic moieties [6].

Polysaccharides/silica hybrids prepared through the sol–gel method have been studied as models for a new generation of hybrid silica-based materials for several applications [7]. Nevertheless, due to the poor compatibility between the sol system and natural biopolymers, the formation of polysaccharides/silica hybrid materials is not a trivial task. Some polysaccharides can be more easily incorporated into sol–gel processes than others. The most commonly used polysaccharides have been chitosan [8, 9], alginate [10, 11], and cellulose [12, 13]. So far, few studies have been reported on preparing hybrid polysaccharide-silica materials using carrageenan [14].

Over the last few years, we have reported a series of silica-polysaccharide hybrid materials that use alkoxysilane-modified biopolymers as precursors in a new sol–gel method [15–18]. This sol–gel method has also been explored to coat magnetic iron oxide cores with hybrid silicious shells, thus providing a series of functional materials for magnetic-assisted environmental and medical nanotechnologies [18–22]. Noteworthy, the surfaces of the ensuing magnetic nanomaterials have specific chemical functionalities provided by the biopolymer, which are instrumental for capturing target species, such as in water-cleaning nanosorbents and in biomolecule immobilization substrates. Hence, the magnetic hybrids effectively removed several emerging pollutants, namely pharmaceuticals (diclofenac, naproxen, ketoprofen, sulfamethoxazole, and ciprofloxacin) [19, 23–25] and pesticides (glyphosate) [18], with high adsorption capacity, reusability and applicability in natural water samples. Moreover, a drug delivery system comprising an antitumor agent (doxorubicin) loaded magnetic hybrids for anticancer therapy were developed and opens the way towards the development of theranostic agents [21]. Another study showed the application of magnetic silica hybrids in the purification of an Immunoglobulin (IgG) seemed to have high potential as a new downstream platform for biologically active biomolecules [22]. Modification with TM provides a new way to expand the multifunctionality of such hybrid materials, yet this strategy remains unexplored. For this reason, the main goal of this research was to investigate the in situ sol–gel modification with TM of carrageenan-silica hybrids, which is a straightforward method and takes advantage of the chemistry employed in the fabrication of silica-polysaccharide materials.

2 Experimental part

2.1 Chemicals

Ethanol (CH_3CH_2OH) (>99%) was obtained from Panreac and methanol (CH_3OH) (>99%) was purchased from VWR. Tetraethyl orthosilicate ($Si(OC_2H_5)_4$, TEOS, >99%) and 3-(triethoxysilyl)propyl isocyanate ($((C_2H_5O)_3Si(CH_2)_3NCO$, ICPTES, 95%) were purchased from Sigma-Aldrich. N,

N-dimethylformamide ($HCON(CH_3)_2$) was obtained from Carlo Erba Reagents, and ammonia solution (NH_4OH, 25% NH_3) was purchased from Riedel-de-Häen. κ- carrageenan (300.000 g mol^{-1}) was obtained from Fluka Chemie. Cobalt (II) chloride hexahydrate ($CoCl_2.6H_2O$) (98%), copper (II) acetate monohydrate ($Cu(CH_3COO)_2.H_2O$) (99%) and zinc acetate dihydrate ($Zn(CH_3COO)_2.2H_2O$) were purchased from Panreac. Nickel (II) chloride hexahydrate ($NiCl_2.6H_2O$) (99%) was obtained from Sigma-Aldrich. Ultra-pure water used was obtained using a Milli-Q system with a 0.22 µm filter (Synergy equipment, Millipore).

2.2 Synthesis of the κ-carrageenan precursor (SiκCRG)

An alkoxysilane containing κ-carrageenan (SiκCRG) covalently linked was prepared by reacting the biopolymer with the silane coupling agent ICPTES, following a procedure that was previously reported by us [15]. The reaction was performed in a deprotonated solvent (N, N- dimethylformamide) (DMF). Typically, SiκCRG resulted from the reaction between dry κ-carrageenan (1 g), dry DMF (13 mL), and the silane coupling agent ICPTES (1.3 mL). The synthesis was performed in a dried atmosphere at 100 °C, under solvent reflux conditions, and left under constant stirring for 24 h. The SiκCRG was washed several times with dry methanol and dry ethanol and finally dried at room temperature.

2.3 Synthesis of the TM-modified κ-carrageenan-silica hybrid particles

The hybrid materials were obtained by hydrolysis and condensation of a mixture of the SiκCRG with a silica precursor (TEOS) in ethanol containing ultra-pure water and a TM salt solution, using a base as a catalyst. Cobalt (II) chloride hexahydrate ($CoCl_2{\cdot}6H_2O$), copper (II) acetate monohydrate ($Cu(CH_3COO)_2{\cdot}H_2O$), zinc acetate dihydrate ($Zn(CH_3COO)_2{\cdot}2H_2O$) and nickel (II) chloride hexahydrate ($NiCl_2{\cdot}6H_2O$) were used as TMs source. Briefly, the SiκCRG (0.3 g) and TEOS (0.406 mL) were mixed with deionized water (0.9 mL). Then, the TM aqueous solution (0.09 mL, 0.1 M) was added, with ethanol (8.5 mL) and ammonia solution (0.15 mL), under constant stirring (250 rpm). The synthesis was maintained over 24 h, at room temperature. Then, the hybrid particles were washed five times with deionized water and once with dry ethanol, followed by centrifugation. Finally, the solvents were evaporated, and the TM-modified κ-carrageenan-silica hybrid particles were obtained (Fig. S1, Supporting Information). In view of the results obtained in this work, the materials are denominated as SiO_2/SiκCRG/Co, SiO_2/SiκCRG/Cu, SiO_2/SiκCRG/Ni, and SiO_2/SiκCRG/Zn, taking into account the TM salt solution used. For comparative purposes, TM-modified silica (SiO_2) particles have also been [26] prepared by using the Stöber method in the presence of each TM salt solution, to generate SiO_2/Co, SiO_2/Cu, SiO_2/Ni, and SiO_2/Zn particles.

2.4 Instrumentation

Fourier transform infrared (FTIR) spectra of the particles were measured in the solid state. The spectra of the materials were collected using a Bruker Optics Tensor 27 spectrometer coupled to a horizontal attenuated total reflectance (ATR) cell, using 256 scans at a resolution of 4 cm^{-1}. The elemental analysis of carbon, nitrogen, hydrogen, and sulfur was obtained on a Leco Truspec-Micro CHNS 630-200-200. The specific surface area of the particles was assessed by nitrogen adsorption Brunauer–Emmett–Teller (BET) measurements, performed with a Gemini V2.0 Micromeritics instrument. The pore volume was evaluated from the adsorption branch using the Barret–Joyner–Halenda method. The morphology and size of the particles were analyzed by scanning electron microscopy (SEM) using a Hitachi SU-70 instrument operated at an accelerating voltage of 15 kV and by scanning transmission electron microscopy (STEM), using a 200 kV Hitachi HD-2700 STEM microscope equipped with energy-dispersive X-ray spectroscopy (EDS) and secondary electron detectors. Samples for SEM analysis were prepared by placing an aliquot of a dilute suspension of the particles in ethanol over a glass slide glued to the sample holder using double-sided carbon tape, and then coating the sample with carbon sputtering. Samples for STEM analysis were prepared by evaporating the diluted suspensions of the particles on a grid coated with an amorphous carbon film. Thermogravimetric analysis (TGA) of the materials was performed by using a TGA 50 instrument from Shimadzu. Samples were heated from 25 to 900 at 10 °C min^{-1} under a nitrogen atmosphere. The ^{29}Si MAS/CP MAS NMR and ^{13}C CP MAS NMR spectra were recorded on a Bruker Avance III 400 MHz (9.4 T) spectrometer at 79.49 and 100.61 MHz, respectively. ^{29}Si MAS/CP MAS NMR spectra were recorded with 4.5 µs ^{1}H 90° pulses, a recycle delay of 60 s, at a spinning rate of 5 kHz and using a probe for a rotor with a diameter of 4 mm. ^{13}C CP/MAS NMR spectra were recorded with 3.65 µs ^{1}H 90° pulses, 1.5 ms contact time, a recycle delay of 5 s, and at a spinning rate of 9 kHz. Diffuse reflectance UV–VIS spectra of the powder samples were recorded on a Jasco U-560 UV/VIS spectrophotometer. The surface charge of the materials was assessed by zeta potential measurements, using a Zetasizer Nano series equipment from Malvern Instruments. The content of the transition metals was determined using inductively coupled plasma-optical emission spectroscopy (ICP-OES) using a model Horiba Jobin Yvon Activa M.

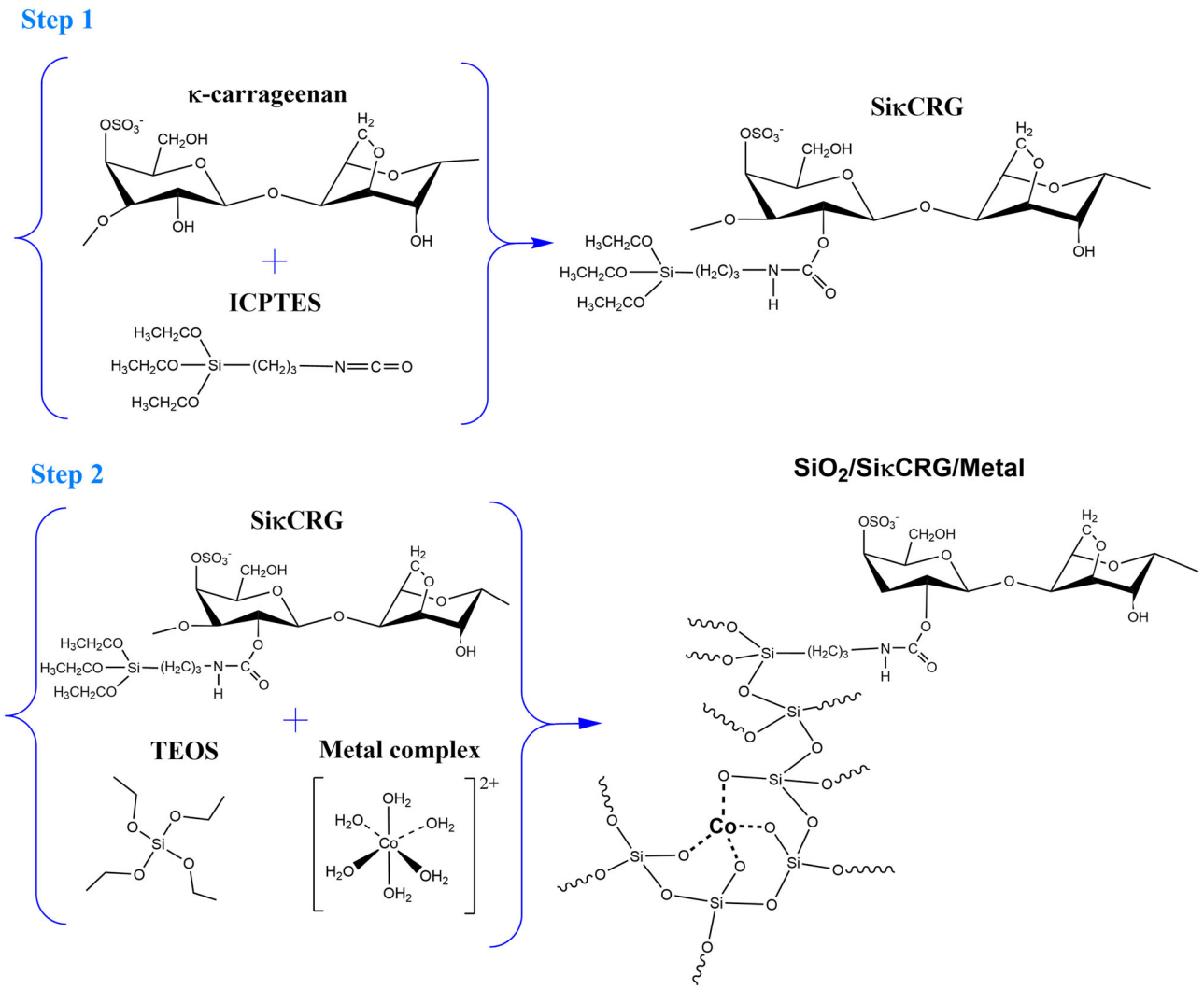

Fig. 1 Schematic representation of the synthesis of the hybrid precursor, SiκCRG (step 1) by reaction of the hydroxyl groups of κ-carrageenan with isocyanate groups of ICPTES. The scheme also illustrates the case of Co-modified hybrid siliceous materials using TEOS in the presence of aqueous solutions of the selected TM ion (step 2), suggesting a coordination environment for the cation

3 Results and discussion

The first step of this work involved the preparation of a hybrid precursor (SiκCRG) by reaction of κ-carrageenan with a functionalized alkoxysilane containing isocyanate groups. Covalent urethane bonds (−NHCOO−) can be formed between the hydroxyl groups of κ-carrageenan with the isocyanate groups (−NCO) of the silane coupling agent ICPTES (Fig. 1). In order to obtain TM-modified κ-carrageenan-silica hybrid particles, in a second step, the SiκCRG and TEOS were mixed, in the presence of aqueous solutions of selected TM ions (TM = Co^{2+}, Cu^{2+}, Ni^{2+}, Zn^{2+}) (Fig. 1). For the sake of comparison, a similar method was applied for preparing the TM-modified SiO_2 based counterparts, i.e., in the absence of the κ-carrageenan containing precursor.

The synthesized particles were analyzed using ATR FTIR spectroscopy (Fig. 2). The spectra of amorphous SiO_2 and TM-modified SiO_2 particles (Fig. S2, Supporting Information) show the typical absorption bands at 429–434 cm^{-1} and 945–946 cm^{-1}, which are assigned to the O–Si–O deformation and stretching vibrations of silanol (Si–OH) surface groups, respectively [27]. The absorption bands at 789–794 cm^{-1} and 1043–1050 cm^{-1} are ascribed to the symmetric and antisymmetric Si–O–Si stretching vibrations, respectively [28, 29]. The vibrations of Co–O (661–570 cm^{-1}) [30], Cu–O (617 cm^{-1}) [31], Ni–O (578–518 cm^{-1}) [32] and Zn–O (468 cm^{-1}) [33] that usually appear within the range of 400–670 cm^{-1}, can barely be seen in the FTIR spectra due to the lower concentration of each TM and presence and overlap of silica peaks that mask these specific vibrations. Regarding the TM-modified hybrid particles (Fig. 2), the FTIR spectral bands of the particles have confirmed the main characteristics of silicate network grafted to κ-carrageenan. Briefly,

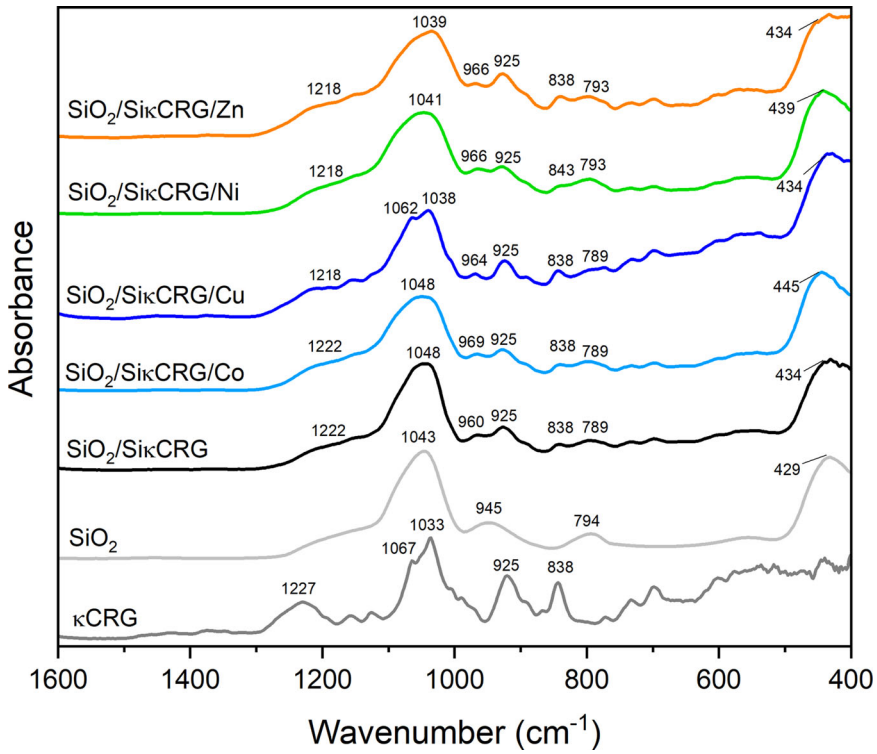

Fig. 2 ATR-FTIR spectra of κCRG, SiO_2, SiO_2/SiκCRG, SiO_2/SiκCRG/Co, SiO_2/SiκCRG/Cu, SiO_2/SiκCRG/Ni and SiO_2/SiκCRG/Zn particles

Table 1 Compositional and structural properties of as-synthesized materials

Sample	C (%)[a]	H (%)[a]	N (%)[a]	S (%)[a]	D (nm)[b]	S_{BET} ($m^2\ g^{-1}$)[c]	V_p ($cm^3\ g^{-1}$)[c]
SiO_2	0.3	1.5	0.4	–	131 ± 9	52.0	0.15
SiO_2/Co	0.9	1.3	0.4	–	6 ± 1	23.4	0.03
SiO_2/Cu	0.8	1.2	0.9	–	60 ± 20	20.1	0.02
SiO_2/Ni	1.0	1.4	0.1	–	13 ± 2	29.2	0.04
SiO_2/Zn	1.6	1.6	1.0	–	180 ± 20	31.3	0.04
SiO_2/SiκCRG	19.5	4.0	0.9	2.3	460 ± 30	9.2	0.015
SiO_2/SiκCRG/Co	15.5	4.1	0.4	2.2	1300 ± 100	3.5	0.005
SiO_2/SiκCRG/Cu	12.2	3.8	0.3	1.0	1100 ± 100	3.9	0.005
SiO_2/SiκCRG/Ni	12.9	3.5	0.3	1.0	1000 ± 200	0.2	0.001
SiO_2/SiκCRG/Zn	21.5	3.6	0.3	3.7	750 ± 50	2.6	0.004

[a]Carbon, hydrogen, nitrogen and sulfur content measured by elemental microanalysis

[b]Particle diameter assessed by TEM

[c]BET specific surface area (S_{BET}) and porosity volume (V_p) assessed by N_2 adsorption

κ-carrageenan spectrum showed typical bands in the region 1067–1033 cm^{-1} due to C–O and C–OH vibrations, a band at 838 cm^{-1} that is attributed to the α(1-3)-D-galactose C–O–S stretching vibration, a band at 925 cm^{-1} that corresponds to the 3,6-anhydro-D-galactose and a broad band at 1227 cm^{-1} due to the S–O antisymmetric stretching of the ester sulfate groups [19]. The typical vibration bands of SiO_2 and κ-carrageenan have also been observed in the spectra of the TM-modified hybrid particles, although these particles have not shown any noticeable changes in the FTIR spectral bands position after being modified with TM.

The organic-inorganic hybrid nature of the TM-modified siliceous materials obtained by this sol–gel method was confirmed by elemental microanalysis (Table 1). While SiO_2 and TM-modified silica particles show low carbon content (<1.6 wt%), all the TM-modified hybrid particles exhibit higher carbon content (>12 wt%), which is in agreement with the formation of hybrids with a significant content of κ-carrageenan as the organic component. The specific surface area (S_{BET}) and pore volume (V_p) of these materials (Table 1) were assessed by nitrogen adsorption/desorption isotherms. The specific surface area decreased from 52.0 $m^2\ g^{-1}$ in SiO_2 to 9.2 $m^2\ g^{-1}$ in SiO_2/SiκCRG, due to the increase of the particle

size and the formation of the hybrid. Identical correlation between the particle size and the surface area was found in the TM-modified hybrids. The BET-specific surface area decreased from 9.2 $m^2 g^{-1}$ (SiO_2/SiκCRG) to values in the range from 0.2 to 3.9 $m^2 g^{-1}$, along with an increase in particle size. The presence of the TM cations during the synthesis of the particles contributed to the surface area decrease [34]. Regarding the inorganic silica particles, the BET-specific surface area decreased from 52.0 $m^2 g^{-1}$ in SiO_2 to values in the range 20.1–31.3 $m^2 g^{-1}$ in modified silica. Since the particle size decreased after modification (except for SiO_2/Zn), the decrease in surface area was most likely due to the blocking of some pores by the TM cations that could limit the adsorption of the probe gas (N_2) inside the pores [35]. The decrease in the pore volume is in agreement with this effect.

The morphological characteristics of the TM-modified and unmodified materials were investigated by SEM (Fig. 3). The SEM analysis showed that unmodified bulk SiO_2 and SiO_2/SiκCRG samples have both uniform and spheroidal particle morphology (Fig. 3a, b). As shown in Table 1, the average size of the SiO_2 particles was 131 ± 9 nm, and decreased to 60 ± 20 nm, 13 ± 2 nm, and 6 ± 1 nm, for the SiO_2/Cu, SiO_2/Ni and SiO_2/Co particles, respectively (Fig. 3c, e and g). Compared with the unmodified SiO_2, the average size of the TM-modified SiO_2 particles markedly decrease, suggesting that the incorporation of the TM cations, such as Co^{2+}, Cu^{2+}, and Ni^{2+}, limits the growth of the SiO_2 particles. Interestingly, the above observation follows the decreasing tendency of the TM ionic radii for the respective coordination geometry, which might suggest a charge density effect of the TM ions when already interacting with the silica oligomers. In the case of SiO_2/Zn particles, as compared to the unmodified SiO_2 sample, the average particle size increased to 180 ± 20 nm, but the particles show a distinct nanoplatelets-like morphology (Fig. 3i) instead of a spheroidal morphology [36, 37]. The TM-modified κ-carrageenan silica particles (Fig. 3d, f, h and j) presented well-defined spheroidal shape with an average size ranging between 750 nm and 1300 nm in diameter (Table 1). Furthermore, there is not a clear trend on the effect of the TM cation employed on the final average particle size of the modified hybrid materials. These observations are a strong indication of the important role of the alkoxysilane-modified polysaccharide precursor during the sol–gel process, namely by providing diverse oxygen donor groups for coordinating TM cationic species present in the reacting mixture, such as sulfate groups. It should be stressed that the above sol–gel route led to morphological uniform spherical particles of the TM-modified hybrid materials without surfactants and emulsions.

XRD patterns of the unmodified and TM-modified particles are shown in Fig. S3 (Supporting Information). For all the materials, the only broad peak detected is the one ascribed to amorphous silica at $2\theta \approx 21°$.

The surface charge measured as zeta-potential revealed a negative surface charge for all the silica and hybrid particles (Table 2). The zeta potential of unmodified SiO_2 and SiO_2/SiκCRG particles was negative (−46 and −68 mV, respectively). The TM-modified κ-carrageenan silica particles presented more negative zeta-potential values, compared with amorphous inorganic SiO_2, indicating that the anionic polysaccharide κ-carrageenan was bonded to the silica network.

A first indication of the presence of the TM cations in the silicious network was their characteristic color, which remained after thoroughly washing the solid samples (Fig. 4). This aspect was further investigated by diffuse reflectance visible (DR-UV/VIS) spectroscopy, as shown in Fig. 4. Overall, the DR-UV/VIS spectra show the absorption features in the visible region as expected for *d–d* electronic transition bands for the respective coordinated TM cations (Fig. 4a–c), except for the Zn^{2+} samples in which the metal has the *d* orbitals totally filled (Fig. 4d). Furthermore, the DR-UV/VIS spectra suggest different coordination environments for the TM cations in the hybrid materials. The analysis of the spectra for the Co-modified siliceous materials (SiO_2/Co and SiO_2/SiκCRG/Co) is particularly instructive because it showed bands peaked at 527, 584, and 643 nm, which is a triplet characteristic of Co^{2+} in a tetrahedral environment [38–40], thus in agreement with the observed blue color of the respective samples (Fig. 4a). It is known that Co^{2+} changes in color from pink to blue, from octahedral coordination in the corresponding hydrated samples to tetrahedral coordination in the dehydrated samples [39, 40]. Additionally, the DR-UV/VIS spectra of Cu-modified silica (SiO_2/Cu) and hybrid (SiO_2/SiκCRG/Cu) materials (Fig. 4b) show two bands at around 330–350 nm, that can be ascribed to charge transfer between mononuclear Cu^{2+} ion and oxygen and between Cu^{2+} and oxygen in oligonuclear $[Cu–O–Cu]_n$ surface species [41]. The band in the 600–800 nm range is usually attributed to *d–d* transitions of the Cu^{2+} ions in an octahedral or tetragonal distorted octahedral surrounding [42]. These results are in agreement with the structures proposed in refs. [43–45], showing the typical fingerprint of hexacoordinated Cu^{2+} ions. Figure 4c shows the DR-UV/VIS spectra of Ni-modified silica and hybrid materials. For these materials, two bands located between 401 and 680 nm are observed, corresponding to the *d–d* transitions of the Ni^{2+} cations [46–48], indicating an octahedral coordination of Ni^{2+} [49]. Figure 4d shows the DR-UV/VIS spectra of Zn-modified silica (SiO_2/Zn) and hybrid (SiO_2/SiκCRG/Zn) particles, which are in agreement with other studies reported in the literature for Zn-modified silica particles [50]. Although the above interpretation is consistent with the data available, a

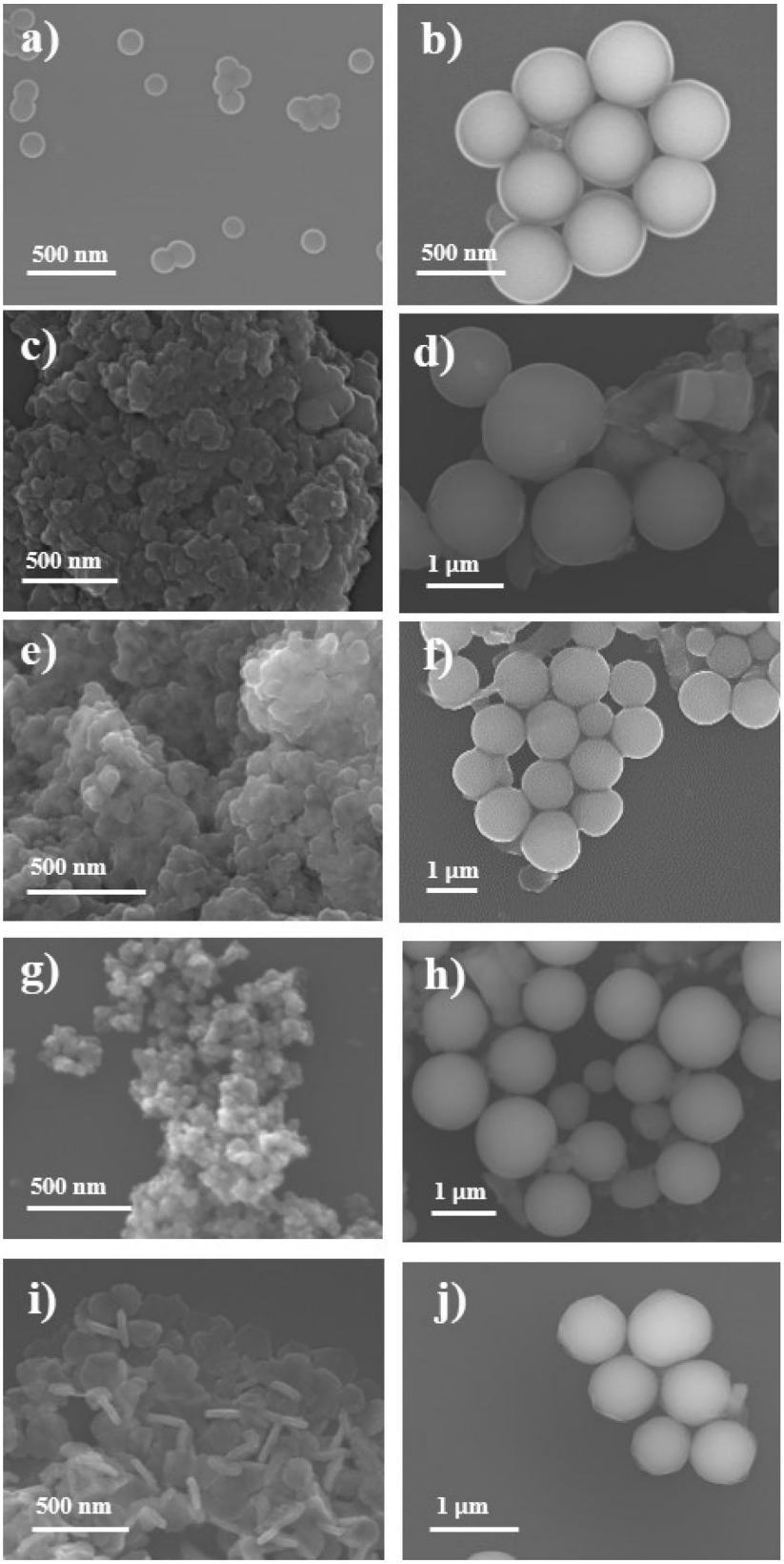

Fig. 3 SEM images of particles in dry and powdered samples obtained by sol–gel routes: **a** SiO_2, **b** SiO_2/SiκCRG, **c** SiO_2/Co, **d** SiO_2/SiκCRG/Co, **e** SiO_2/Cu, **f** SiO_2/SiκCRG/Cu, **g** SiO_2/Ni, **h** SiO_2/SiκCRG/Ni, **i** SiO_2/Zn, and **j** SiO_2/SiκCRG/Zn

detailed description of the type of coordination environments of the TM cations in the silicious shells is still an open issue.

To determine the TM content, the modified materials were analyzed by ICP-OES. The ICP-OES results showed that TM-modified particles contain between 0.2 and 2.8% of metal (Table S1, Supporting Information), which corroborates the results previously discussed and indicates the presence of the TM cations in the silicious network of the materials.

Table 2 Zeta potential of the hybrid particles in aqueous suspensions at pH 7

Sample	Zeta Potential (mV)
SiO_2	–46 ± 1
SiO_2/SiκCRG	–68 ± 3
SiO_2/Cu	–53.0 ± 0.4
SiO_2/SiκCRG/Cu	–52 ± 2
SiO_2/Co	–51 ± 1
SiO_2/SiκCRG/Co	–51.0 ± 0.9
SiO_2/Ni	–52.1 ± 0.6
SiO_2/SiκCRG/Ni	–53.0 ± 0.6
SiO_2/Zn	–49.6 ± 0.2
SiO_2/SiκCRG/Zn	–62 ± 1

The above electronic spectra indicate that TM ions have been successfully incorporated into the silica matrix. However, this has been further confirmed by energy-dispersive EDS and STEM performed on the samples (Figs. 5 and S4, Supporting Information). The EDS maps show a homogeneous dispersion of the TM ions over the particles for all the samples analyzed. The EDS Si signal provides maps with a higher color density than the TM EDS signals, which is consistent with the dispersion of the metal species on the siliceous matrix.

Solid-state ^{29}Si NMR spectroscopy of the powders was explored to investigate the effect of TM modification on the degree of condensation of the silica network. Figure 6 shows the cross-polarization (CP)/magic-angle spinning (MAS) ^{29}Si NMR spectra; the corresponding chemical-shift assignments are listed in Table S2 (Supporting Information). The silicon sites are labeled according to the usual NMR spectroscopy notation: Q^n represents quaternary Si atoms linked to n siloxane groups and $(4 - n)$ OH groups [51–53]. Figure 6a shows the ^{29}Si MAS NMR spectra of bulk SiO_2 and the TM-modified silica particles and Fig. 6b shows the ^{29}Si MAS NMR spectra of the SiO_2/SiκCRG hybrid and the TM-modified κ-carrageenan SiO_2 particles and yields information on the connectivity of the siloxane bonds. Bulk SiO_2 particles (Fig. 6a) show two main signals at −111 and −102 ppm, attributed to the silica sites and

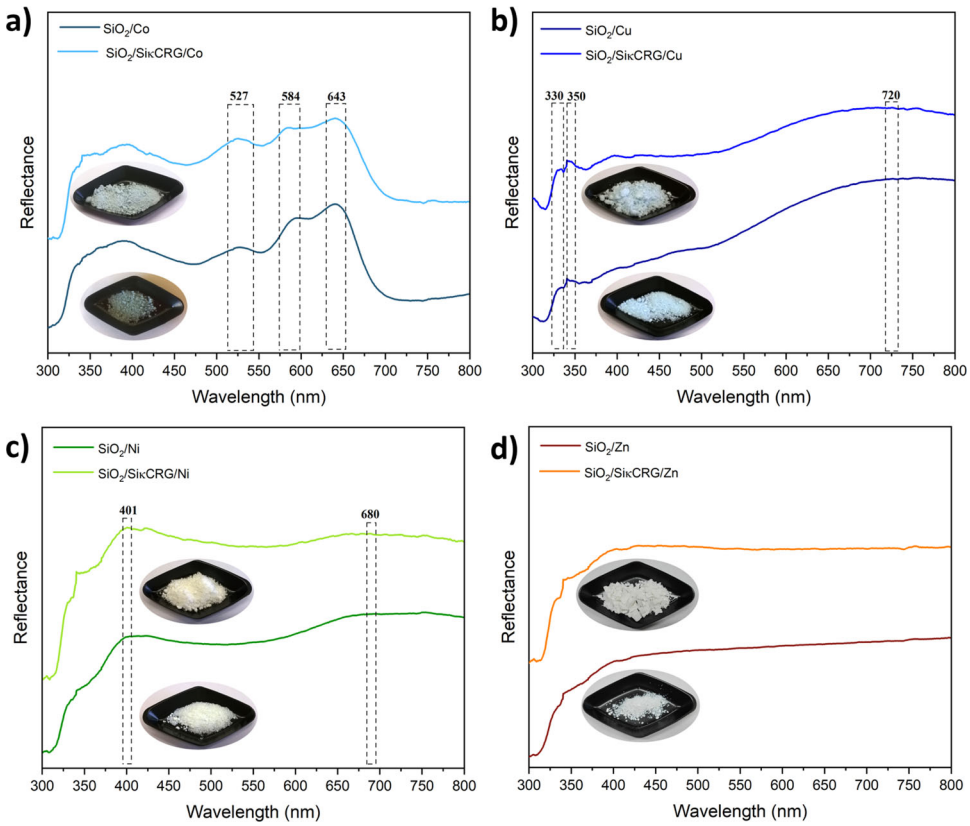

Fig. 4 Diffuse reflectance UV/VIS spectra of TM-modified silica (SiO_2/Co, SiO_2/Cu, SiO_2/Ni, and SiO_2/Zn) and hybrid (SiO_2/SiκCRG/Co, SiO_2/SiκCRG/Cu, SiO_2/SiκCRG/Ni, and SiO_2/SiκCRG/Zn) materials and photographs of the powdered samples

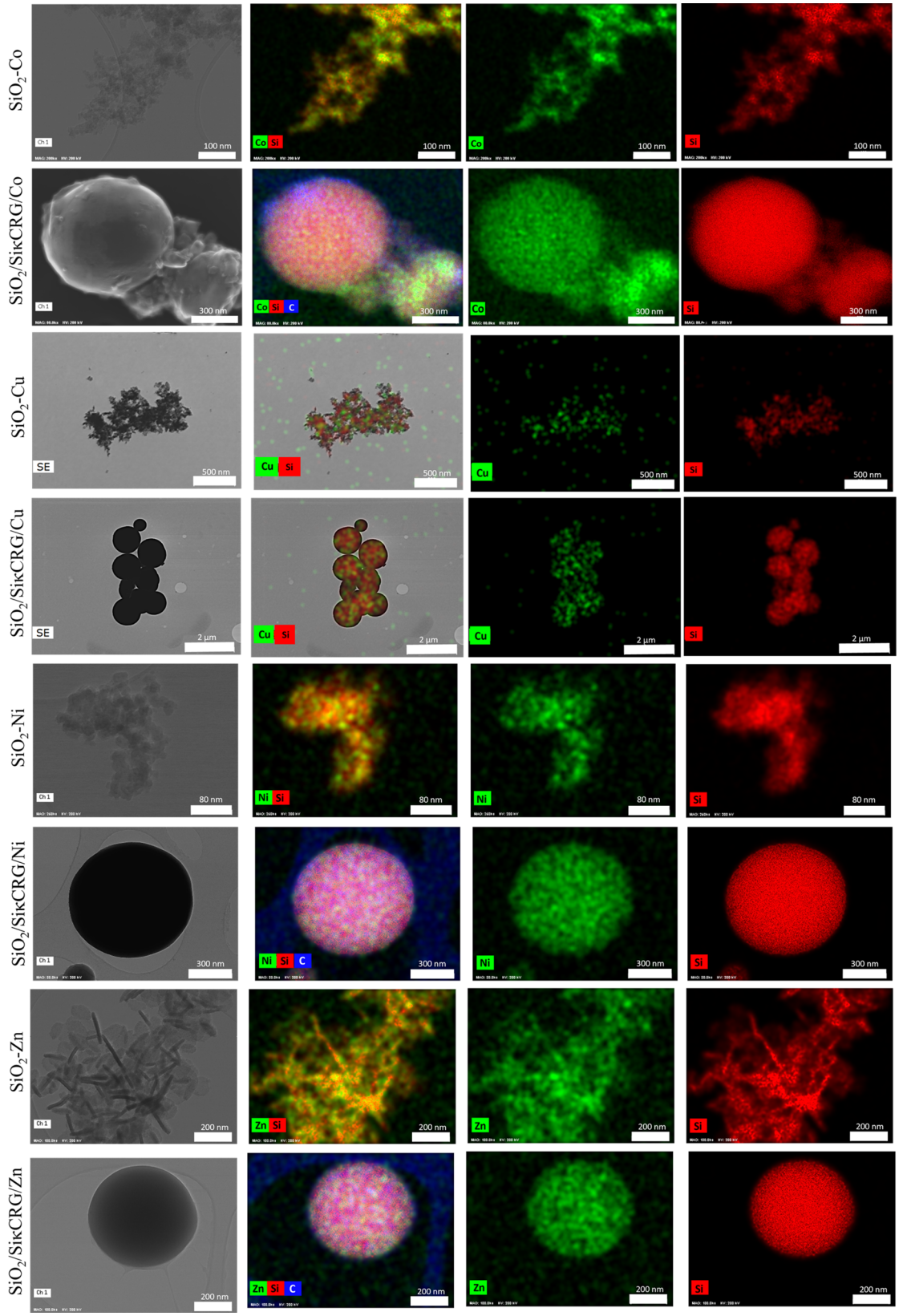

Fig. 5 STEM images of SiO_2/Co, SiO_2/SiκCRG/Co, SiO_2/Cu, SiO_2/SiκCRG/Cu, SiO_2/Ni, SiO_2/SiκCRG/Ni, SiO_2/Zn, and SiO_2/SiκCRG/Zn particles, and elemental mapping of Co, Cu, Ni, and Zn

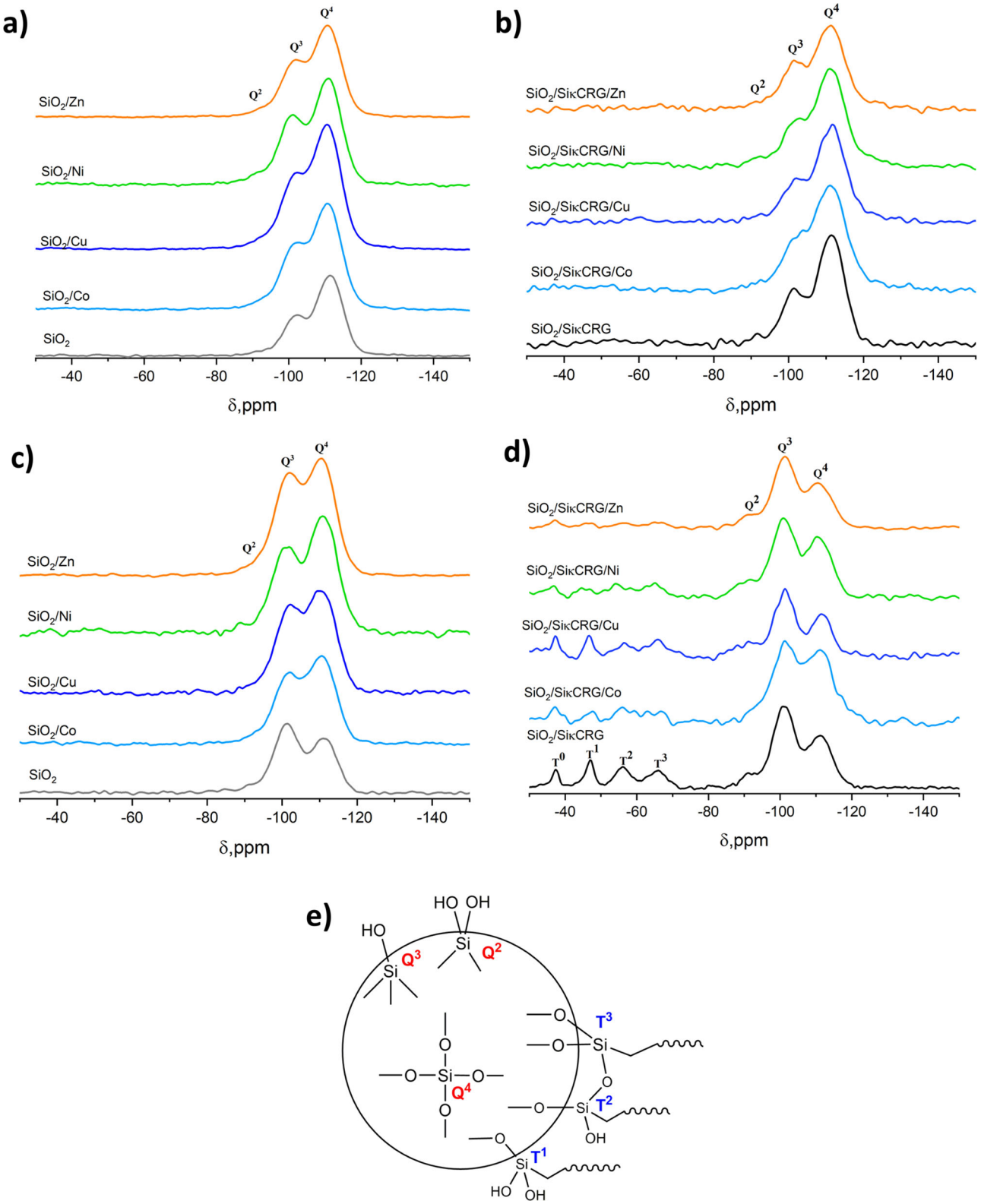

Fig. 6 ^{29}Si MAS NMR spectra of **a** TM-modified silica particles and **b** TM-modified hybrid silica particles. ^{29}Si CP/MAS NMR spectra of **c** TM-modified silica particles and **d** TM-modified hybrid silica particles; and **e** schematic representation showing the labeling of Si sites according to NMR spectroscopy notation usually applied to silica networks

the unreacted surface silanol sites, respectively [51]. The chemical shifts between −90.6 ppm and −111.2 ppm in SiO_2 were ascribed to geminated silanols Q^2 ($Si(OSi)_2(OH)_2$), isolated silanols Q^3 ($Si(OSi)_3OH$) and siloxane bridges Q^4 $Si(OSi)_4$, respectively [52]. The fraction of silanol groups $[(Q^2 + Q^3)/Q^4]$ that can be calculated from the ^{29}Si MAS NMR spectra was 0.50 in SiO_2 particles and decreased to 0.44 in the SiO_2/SiκCRG hybrid (Table S2, Supporting Information). The covalent bonding of the hybrid precursor SiCRG on the surface of the particles was supported by the decrease in the number of surface hydroxyl groups. Moreover, the fraction of silanol groups was 0.52, 0.50, 0.60, and 0.53 in SiO_2/Co, SiO_2/Cu, SiO_2/Ni, and SiO_2/Zn particles, respectively, and decreased to 0.37, 0.33, 0.36 and 0.43 in SiO_2/SiκCRG/Co, SiO_2/SiκCRG/Cu, SiO_2/SiκCRG/Ni, and SiO_2/SiκCRG/Zn particles, respectively. SiO_2/SiκCRG/Co, SiO_2/SiκCRG/Cu, SiO_2/SiκCRG/Ni, and SiO_2/SiκCRG/Zn showed chemical shifts at −103.9, −102.1, −103.1, and −101.4 ppm respectively, which might be imposed by the formation of Si–O–TM bridges involving the Q^3 silicon units [54]. The SiO_2/SiκCRG/Co, SiO_2/SiκCRG/Cu, SiO_2/SiκCRG/Ni, and SiO_2/SiκCRG/Zn samples show Q^4 resonances at −111.1, −111.7, −111.2, and −111.4 ppm, respectively. Furthermore, as compared to the unmodified samples, broadening of the Q^3 and Q^4 peaks (Fig. 6b) occurs, which is due to the presence of TM ions in the silica matrix.

Comparing the ^{29}Si CP MAS NMR spectra of SiO_2 materials (Fig. 6c) with the ^{29}Si CP MAS NMR spectra (Fig. 6d) of the SiO_2/SiκCRG/TM materials show a decrease in the intensity of the Q^4 signals comparing with the intensity of the Q^3 signals, which means that the modified hybrid materials have an increased number of SiOH% content, i.e., the amount of Q^3. In addition, four new signals appear at −37.4, −47.1, −56.1, and −65.8 ppm which, compared to literature values, can be ascribed to T^0, T^1, T^2, and T^3 Si sites, where *n* denotes the number of –Si–O– bonds linked to the Si site T^n [15]. Thus, T^1, T^2, and T^3 represent the Si sites in $RSi(OSi)(OH)_2$, $RSi(OSi)_2OH$, and $RSi(OSi)_3$, respectively [R = –$(CH_2)_3$ –NHCOO –κ-carrageenan] and further support the polysaccharide κ-carrageenan's covalent attachment to the siliceous network. The presence of T^0 [$RSi(OH)_3$] indicates that the hydrolysis of the alkoxy groups of the κ-carrageenan precursor can occur during the sol–gel reaction. The ^{29}Si CP MAS NMR spectra of SiO_2/SiκCRG/Co, SiO_2/SiκCRG/Cu, SiO_2/SiκCRG/Ni, and SiO_2/SiκCRG/Zn show four new signals corresponding to Si sites in T^0, T^1, T^2, and T^3, confirming the formation of the covalent bonding between the κ-carrageenan and the SiO_2 matrix, even in the presence of the selected TM ions.

Further insight into the hybrid composition was provided by ^{13}C CP/magic-angle spinning (MAS) NMR. The ^{13}C CP/MAS NMR spectra of κ-carrageenan, and hybrid particles are shown in Fig. 7a and the chemical shifts are listed in Table S3 (Supporting Information). The spectrum of the hybrid SiO_2/SiκCRG, when compared to κ-carrageenan spectrum, shows new signals at $\delta = 9.6$, 23.1, and 43.6 that correspond to C10, C9, and C8 carbon atoms, respectively, of the Si-bonded propyl chain (Fig. 5b) [51]. Additionally, a new signal that is attributed to the carbon in urethane groups (C7) occurs at $\delta = 157.2$ ppm, demonstrating the covalent bond between the polysaccharide κ-carrageenan and the siliceous network [15]. Although less intense, these new signals are also present in the ^{13}C CP/MAS NMR spectra of the TM-modified hybrid siliceous materials. In addition, the broad resonances between $\delta = 61$ and 106 ppm have been attributed to the skeleton carbon atoms of κ-carrageenan (C1–C6 and C1′–C6′), according to the literature [53].

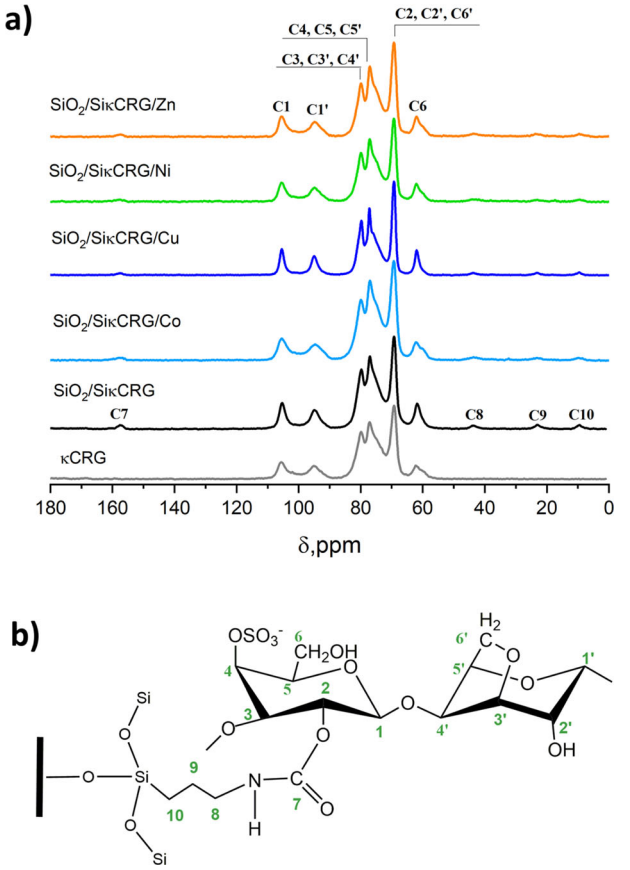

Fig. 7 **a** ^{13}C CP/MAS NMR spectra of κ-carrageenan, SiO_2/SiCRG, SiO_2/SiCRG/Co, SiO_2/SiCRG/Cu, SiO_2/SiCRG/Ni and SiO_2/SiCRG/Zn particles; and **b** chemical structure, with carbons numbered, of SiO_2/SiκCRG hybrid

Thermogravimetric analysis (TGA) measurements were performed to evaluate the thermal properties of the materials. Figure 8a shows the TGA of bulk silica and TM-modified silica particles. The weight loss of bare silica below 200 °C is 4% which is attributed to the physisorbed water [55], and the mass loss from 200 to 600 °C is related

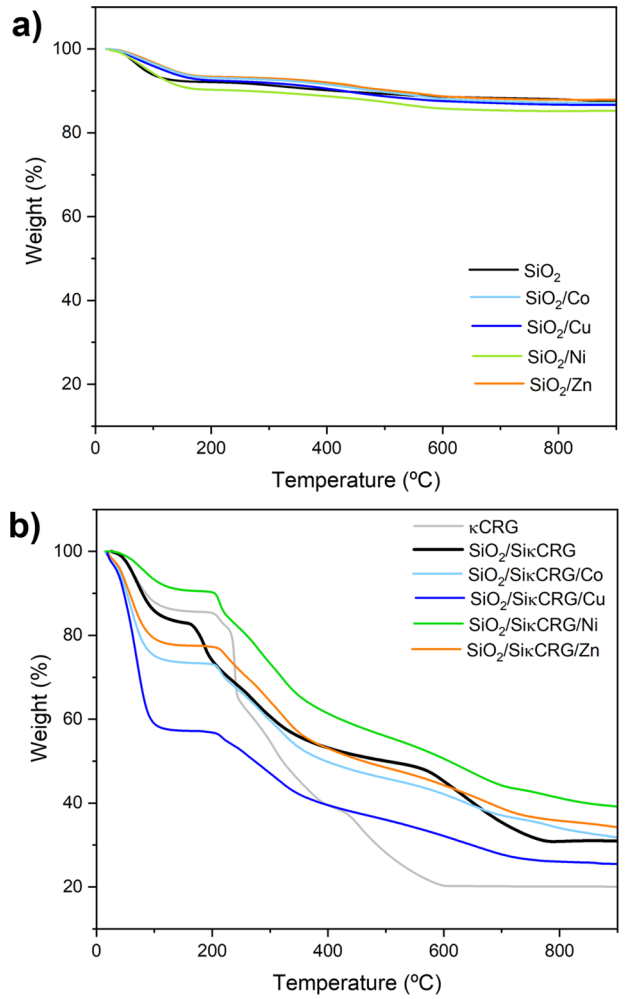

Fig. 8 TGA curve of **a** SiO_2, SiO_2/Co, SiO_2/Cu, SiO_2/Ni, SiO_2/Zn and **b** κCRG, SiO_2/SiκCRG, SiO_2/SiκCRG/Co, SiO_2/SiκCRG/Cu, SiO_2/SiκCRG/Ni and SiO_2/SiκCRG/Zn, in nitrogen atmosphere

to silica hydroxylation [56]. The polysaccharide κ-carrageenan (Fig. 8b) shows weight loss in three distinct stages: below 200 °C (16% weight loss) corresponds to the loss of adsorbed and bound water; a second stage from 230 to 400 °C (61% weight loss) is due to carbohydrate-backbone fragmentation and sulfur dioxide release [57], and further decomposition at higher temperatures leads to 20% residue at 900 °C, which is due to carbon. The onset temperature of the second stage decreased to 171 °C in the unmodified hybrid (SiO_2/SiκCRG) due to the thermal dissociation of urethane bonds in aliphatic urethane. However, in the TM-modified hybrids, this temperature was higher (210–218 °C), indicating that the TM decreases the resistance to thermal decomposition (Fig. 8b). Overall, the thermal degradation of native κ-carrageenan is faster than that of TM-modified κ-carrageenan silica particles. About 77% weight loss takes place in the temperature range of 400–550 °C for κ-carrageenan. In the SiO_2/SiκCRG, SiO_2/SiκCRG/Co, SiO_2/SiκCRG/Cu, SiO_2/SiκCRG/Ni, and SiO_2/SiκCRG/Zn samples, a weight loss of 52%, 56%, 66%, 47%, and 53%, respectively, was observed at 550 °C. The differences observed in the weight losses by varying the TM not only confirm the presence of the TM ion, but also suggest that the respective structures of the κ-carrageenan backbones might be changed depending on the TM species. At 900 °C the residue was about 30% and 32%, 25%, 39%, and 34% for unmodified SiO_2/SiκCRG and hybrids modified with Co, Cu, Ni, and Zn TM, respectively.

4 Conclusions

TM-modified (TM = Co^{2+}, Cu^{2+}, Ni^{2+}, Zn^{2+}) carrageenan-silica hybrids were synthesized by an in situ sol–gel route that uses as precursor a covalently linked alkoxysilane modified κ-carrageenan. This room-temperature sol–gel method is simpler in reaction conditions and allows spherical, monodispersed sub-micrometer-sized particles to be obtained without the need of surfactants and emulsions. The measured specific surface area of the TM-modified materials is significantly altered as a result of the blocking of some pores by the TM cations, and the pore volume also decreased. Compared with the unmodified SiO_2, the average size of the TM-modified SiO_2 particles markedly decrease, suggesting that the incorporation of the TM cations, such as Co^{2+}, Cu^{2+}, and Ni^{2+}, limits the growth of the SiO_2 particles. Related to the SiO_2/Zn particles, as compared to the unmodified SiO_2 sample, the average particle size increased but the particles present a distinct nanoplatelets-like morphology. The incorporation of TM in the carrageenan-silica particles has not shown a clear trend in the effect of the TM cation employed on the final average particle size of the modified hybrid materials. However, samples with well-defined spheroidal shapes have been obtained. These observations are a strong indication of the important role of the alkoxysilane-modified polysaccharide precursor during the sol–gel process, namely by providing diverse oxygen donor groups for coordinating TM cationic species present in the reacting mixture, such as sulfate groups. These metal-modified hybrid particles will hopefully aid in improving several applications of technological relevance. As a perspective for future structural studies in these hybrid materials, the collection of extended X-ray absorption fine structure signals would enable the type of coordination of the TM cation in the silica shells to be established.

Author contributions Conceptualization: TT; Methodology: TT and SFS; Formal analysis and investigation: SFS, ALD-d-S and TT; Writing—original draft preparation: SFS; Writing—review and editing: SFS, ALD-d-S and TT; Funding acquisition: ALD-d-S and TT; Resources: ALD-d-S and TT; Supervision: ALD-d-S and TT.

Funding This work is financed by Portugal 2020 through European Regional Development Fund (ERDF) in the frame of

CENTRO2020 in the scope of the project BIOMAG, CENTRO-01-0145-FEDER-181268 and in the scope of the project CICECO—Aveiro Institute of Materials, UIDB/50011/2020 & UIDP/50011/2020 & LA/P/0006/2020, financed by national funds through the FCT/MEC (PIDDAC). The NMR spectrometers are part of the National NMR Network (PTNMR) and are partially supported by Infrastructure Project N° 022161 (co-financed by FEDER through COMPETE 2020, POCI and PORL and FCT through PIDDAC). Open access funding provided by FCT|FCCN (b-on).

Compliance with ethical standards

Conflict of interest The authors declare no competing interests.

Publisher's note Springer Nature remains neutral with regard to jurisdictional claims in published maps and institutional affiliations.

References

1. Gin S, Delaye J-M, Angeli F, Schuller S (2021) Aqueous alteration of silicate glass: state of knowledge and perspectives. Npj Mater Degrad 5:42. https://doi.org/10.1038/s41529-021-00190-5
2. Cionti C, Stucchi M, Meroni D (2022) Mimicking stained glass: a hands-on activity for the preparation and characterization of silica films colored with noble metal ions and nanoparticles. J Chem Educ 99:1516–1522. https://doi.org/10.1021/acs.jchemed.1c01141
3. Feng X, Lin L, Duan R et al. (2022) Transition metal ion activated near-infrared luminescent materials. Prog Mater Sci 129:100973. https://doi.org/10.1016/j.pmatsci.2022.100973
4. Zlámalová Cílová Z, Gelnar M, Randáková S (2021) Trends in colouring blue glass in central europe in relation to changes in chemical composition of glass from the middle ages to modern age. Minerals 11:1001. https://doi.org/10.3390/min11091001
5. Downs EE, Ao SS, Siegel RW, Schadler LS (2017) Transition metal doping of amorphous silica particles. J Nanopart Res 19:337. https://doi.org/10.1007/s11051-017-4005-5
6. Yang J-W, Fang W, Williams PN et al. (2020) Functionalized mesoporous silicon nanomaterials in inorganic soil pollution research: Opportunities for soil protection and advanced chemical imaging. Curr Pollut Rep. 6:264–280. https://doi.org/10.1007/s40726-020-00152-6
7. Salama A (2016) Polysaccharides/silica hybrid materials: new perspectives for sustainable raw materials. J Carbohydr Chem 35:131–149. https://doi.org/10.1080/07328303.2016.1154152
8. Liang J-N, Yan L-P, Dong Y-F et al. (2020) Robust and nanostructured chitosan–silica hybrids for bone repair application. J Mater Chem B 8:5042–5051. https://doi.org/10.1039/D0TB00009D
9. Zhao H, Xu J, Wang T (2015) Silica/chitosan core–shell hybrid-microsphere-supported CuI catalyst for terminal alkyne homo-coupling reaction. Appl Catal A Gen 502:188–194. https://doi.org/10.1016/j.apcata.2015.06.016
10. Pannier A, Soltmann U, Soltmann B et al. (2014) Alginate/silica hybrid materials for immobilization of green microalgae Chlorella vulgaris for cell-based sensor arrays. J Mater Chem B 2:7896–7909. https://doi.org/10.1039/C4TB00944D
11. Zhang S, Xu F, Wang Y et al. (2013) Silica modified calcium alginate–xanthan gum hybrid bead composites for the removal and recovery of Pb(II) from aqueous solution. Chem Eng J 234:33–42. https://doi.org/10.1016/j.cej.2013.08.102
12. Guzun AS, Stroescu M, Jinga SI et al. (2014) Plackett–Burman experimental design for bacterial cellulose–silica composites synthesis. Mater Sci Eng: C 42:280–288. https://doi.org/10.1016/j.msec.2014.05.031
13. Xie K, Yu Y, Shi Y (2009) Synthesis and characterization of cellulose/silica hybrid materials with chemical crosslinking. Carbohydr Polym 78:799–805. https://doi.org/10.1016/j.carbpol.2009.06.019
14. Shchipunov YA (2003) Sol–gel-derived biomaterials of silica and carrageenans. J Colloid Interface Sci 268:68–76. https://doi.org/10.1016/S0021-9797(03)00457-0
15. Soares SF, Trindade T, Daniel-da-Silva AL (2015) Carrageenan-silica hybrid nanoparticles prepared by a non-emulsion method. Eur J Inorg Chem 2015:4588–4594. https://doi.org/10.1002/ejic.201500450
16. Soares SF, Fernandes T, Trindade T, Daniel-da-Silva AL (2020) Recent advances on magnetic biosorbents and their applications for water treatment. Environ Chem Lett 18:151–164. https://doi.org/10.1007/s10311-019-00931-8
17. Soares SF, Fateixa S, Trindade T, Daniel-da-Silva AL (2021) A versatile synthetic route towards gelatin-silica hybrids and magnetic composite colloidal nanoparticles. Adv Compos Hybrid Mater https://doi.org/10.1007/s42114-021-00386-y
18. Soares SF, Amorim CO, Amaral JS et al. (2021) On the efficient removal, regeneration and reuse of quaternary chitosan magnetite nanosorbents for glyphosate herbicide in water. J Environ Chem Eng 9:105189. https://doi.org/10.1016/j.jece.2021.105189
19. Soares SF, Nogueira J, Trindade T, Daniel-da-Silva AL (2022) Towards efficient ciprofloxacin adsorption using magnetic hybrid nanoparticles prepared with κ-, ι-, and λ-carrageenan. J Nanostructure Chem https://doi.org/10.1007/s40097-022-00498-x
20. Soares SF, Rocha MJ, Ferro M et al. (2019) Magnetic nanosorbents with siliceous hybrid shells of alginic acid and carrageenan for removal of ciprofloxacin. Int J Biol Macromol 139:827–841. https://doi.org/10.1016/j.ijbiomac.2019.08.030
21. Nogueira J, Soares SF, Amorim CO et al. (2020) Magnetic driven nanocarriers for pH-responsive doxorubicin release in cancer therapy. Molecules 25:333. https://doi.org/10.3390/molecules25020333
22. Magalhães FF, Almeida MR, Soares SF et al. (2020) Recovery of immunoglobulin G from rabbit serum using κ-carrageenan-modified hybrid magnetic nanoparticles. Int J Biol Macromol 150:914–921. https://doi.org/10.1016/j.ijbiomac.2020.02.135
23. Soares SF, Fernandes T, Sacramento M et al. (2019) Magnetic quaternary chitosan hybrid nanoparticles for the efficient uptake of diclofenac from water. Carbohydr Polym 203:35–44. https://doi.org/10.1016/j.carbpol.2018.09.030
24. Soares SF, Trindade T, Daniel-da-Silva AL (2021) Enhanced removal of non-steroidal inflammatory drugs from water by quaternary chitosan-based magnetic nanosorbents. Coatings 11:964. https://doi.org/10.3390/coatings11080964
25. Soares SF, Fernandes T, Trindade T, Daniel-da-Silva AL (2019) Trimethyl chitosan/siloxane-hybrid coated Fe_3O_4 nanoparticles for

the uptake of sulfamethoxazole from water. Molecules 24:1958. https://doi.org/10.3390/molecules24101958
26. Green DL, Lin JS, Lam Y-F et al. (2003) Size, volume fraction, and nucleation of Stober silica nanoparticles. J Colloid Interface Sci 266:346–358. https://doi.org/10.1016/S0021-9797(03)00610-6
27. Viswanathan K (2011) Preparation and characterization of fluorescent silica coated magnetic hybrid nanoparticles. Colloids Surf A Physicochem Eng Asp 386:11–15. https://doi.org/10.1016/j.colsurfa.2011.06.017
28. Digigow RG, Dechézelles J-F, Dietsch H et al. (2014) Preparation and characterization of functional silica hybrid magnetic nanoparticles. J Magn Magn Mater 362:72–79. https://doi.org/10.1016/j.jmmm.2014.03.026
29. Tavares DS, Daniel-da-Silva AL, Lopes CB et al. (2013) Efficient sorbents based on magnetite coated with siliceous hybrid shells for removal of mercury ions. J Mater Chem A Mater 1:8134. https://doi.org/10.1039/c3ta10914c
30. Tang C-W, Wang C-B, Chien S-H (2008) Characterization of cobalt oxides studied by FT-IR, Raman, TPR and TG-MS. Thermochim Acta 473:68–73. https://doi.org/10.1016/j.tca.2008.04.015
31. Cordoba G, Arroyo R, Fierro JLG, Viniegra M (1996) Study of xerogel–glass transition of CuO/SiO_2. J Solid State Chem 123:93–99. https://doi.org/10.1006/jssc.1996.0156
32. Worku AK, Ayele DW, Habtu NG (2021) Influence of nickel doping on MnO_2 nanoflowers as electrocatalyst for oxygen reduction reaction. SN Appl Sci 3:764. https://doi.org/10.1007/s42452-021-04746-7
33. Roy A, Polarz S, Rabe S et al. (2004) First preparation of nanocrystalline zinc silicate by chemical vapor synthesis using an organometallic single-source precursor. Chem Eur J 10:1565–1575. https://doi.org/10.1002/chem.200305397
34. Gupta N, Santhiya D, Murugavel S et al. (2018) Effects of transition metal ion dopants (Ag, Cu and Fe) on the structural, mechanical and antibacterial properties of bioactive glass. Colloids Surf A Physicochem Eng Asp 538:393–403. https://doi.org/10.1016/j.colsurfa.2017.11.023
35. El-Molla SA (2005) Surface and catalytic properties of Cr_2O_3/MgO system doped with manganese and cobalt oxides. Appl Catal A Gen 280:189–197. https://doi.org/10.1016/j.apcata.2004.10.042
36. Abdelmohsen AH, Rouby WMA, el, Ismail N, Farghali AA (2017) Morphology transition engineering of ZnO nanorods to nanoplatelets grafted Mo_8O_{23}-MoO_2 by polyoxometalates: Mechanism and possible applicability to other oxides. Sci Rep 7:5946. https://doi.org/10.1038/s41598-017-05750-x
37. Ye C, Fang X, Hao Y et al. (2005) Zinc oxide nanostructures: Morphology derivation and evolution. J Phys Chem B 109:19758–19765. https://doi.org/10.1021/jp0509358
38. Verberckmoes AA, Weckhuysen BM, Schoonheydt RA (1998) Spectroscopy and coordination chemistry of cobalt in molecular sieves. Microporous Mesoporous Mater 22:165–178. https://doi.org/10.1016/S1387-1811(98)00091-2
39. Bellmann A, Rautenberg C, Bentrup U, Brückner A (2020) Determining the location of Co^{2+} in zeolites by UV-Vis diffuse reflection spectroscopy: a critical view. Catalysts 10:123. https://doi.org/10.3390/catal10010123
40. Neaţu Ş, Puche M, Fornés V, Garcia H (2014) Cobalt-containing layered or zeolitic silicates as photocatalysts for hydrogen generation. Chem Commun 50:14643–14646. https://doi.org/10.1039/C4CC05931J
41. Tsiourvas D, Papavasiliou A, Deze E et al. (2017) A green route to copper loaded silica nanoparticles using hyperbranched poly(ethylene imine) as a biomimetic template: Application in heterogeneous catalysis. Catalysts 7:390. https://doi.org/10.3390/catal7120390
42. Pakharukova VP, Moroz EM, Zyuzin DA et al. (2015) Structure of copper oxide species supported on monoclinic zirconia. J Phys Chem C 119:28828–28835. https://doi.org/10.1021/acs.jpcc.5b06331
43. Velasco MI, Krapacher CR, de Rossi RH, Rossi LI (2016) Structure characterization of the non-crystalline complexes of copper salts with native cyclodextrins. Dalton Trans 45:10696–10707. https://doi.org/10.1039/C6DT01468B
44. Martina K, Calsolaro F, Zuliani A et al. (2019) Sonochemically-promoted preparation of silica-anchored cyclodextrin derivatives for efficient copper catalysis. Molecules 24:2490. https://doi.org/10.3390/molecules24132490
45. Dikhtiarenko A, Villanueva-Delgado P, Valiente R et al. (2016) Tris(bipyridine)metal(II)-templated assemblies of 3D alkali-ruthenium oxalate coordination frameworks: Crystal structures, characterization and photocatalytic activity in water reduction. Polymers 8:48. https://doi.org/10.3390/polym8020048
46. Oliver-Tolentino MA, Vázquez-Samperio J, Manzo-Robledo A et al. (2014) An approach to understanding the electrocatalytic activity enhancement by superexchange interaction toward OER in alkaline media of Ni–Fe LDH. J Phys Chem C 118:22432–22438. https://doi.org/10.1021/jp506946b
47. Martínez-Sánchez C, Regmi C, Lee SW, Rodríguez-González V (2021) Effects of Ce doping on the photocatalytic and electrochemical performance of nickel hydroxide nanostructures. Top Catal 64:73–83. https://doi.org/10.1007/s11244-020-01295-y
48. Ganesh I, Gupta AK, Kumar PP et al. (2012) Preparation and characterization of Ni-doped materials for photocurrent and photocatalytic applications. Sci World J 2012:1–16. https://doi.org/10.1100/2012/127326
49. Umegaki T, Takei C, Watanuki Y et al. (2013) Fabrication of hollow nickel-silica composite spheres using l(+)-arginine and their catalytic performance for hydrolytic dehydrogenation of ammonia borane. J Mol Catal A Chem 371:1–7. https://doi.org/10.1016/j.molcata.2013.01.014
50. Mohamed RM, Barakat MA (2012) Enhancement of photocatalytic activity of ZnO/SiO_2 by nanosized Pt for photocatalytic degradation of phenol in wastewater. Int J Photoenergy 2012:1–8. https://doi.org/10.1155/2012/103672
51. Arantes TM, Pinto AH, Leite ER et al. (2012) Synthesis and optimization of colloidal silica nanoparticles and their functionalization with methacrylic acid. Colloids Surf A Physicochem Eng Asp 415:209–217. https://doi.org/10.1016/j.colsurfa.2012.09.041
52. Babonneau F, Baccile N, Laurent G et al. (2010) Solid-state nuclear magnetic resonance: a valuable tool to explore organic-inorganic interfaces in silica-based hybrid materials. Comptes Rendus Chim 13:58–68. https://doi.org/10.1016/j.crci.2009.08.001
53. van de Velde F, Pereira L, Rollema HS (2004) The revised NMR chemical shift data of carrageenans. Carbohydr Res 339:2309–13. https://doi.org/10.1016/j.carres.2004.07.015
54. Andas J, Adam F, Rahman IAb (2014) Sol–gel derived mesoporous cobalt silica catalyst: synthesis, characterization and its activity in the oxidation of phenol. Appl Surf Sci 315:154–162. https://doi.org/10.1016/j.apsusc.2014.07.118
55. Zhuravlev LT (2000) The surface chemistry of amorphous silica. Zhuravlev model. Colloids Surf A Physicochem Eng Asp 173:1–38. https://doi.org/10.1016/S0927-7757(00)00556-2
56. Berezovska IS, Yanishpolskii VV, Tertykh VA (2008) Synthesis of mesoporous silicas inside large pores of inorganic matrix. J Therm Anal Calorim 94:649–653. https://doi.org/10.1007/s10973-008-9361-z
57. Thommes M, Blaschek W, Kleinebudde P (2007) Effect of drying on extruded pellets based on κ-carrageenan. Eur J Pharm Sci 31:112–118. https://doi.org/10.1016/j.ejps.2007.02.010